Journal of Power Sources 221 (2013) 427–434

Contents lists available at SciVerse ScienceDirect

Journal of Power Sources

journal homepage: www.elsevier.com/locate/jpowsour

# Synthesis of high-capacity Ti- and/or Fe-substituted $Li_2MnO_3$ positive electrode materials with high initial cycle efficiency by application of the carbothermal reduction method

Mitsuharu Tabuchi [a,*], Yoko Nabeshima [a], Tomonari Takeuchi [a], Hiroyuki Kageyama [a], Junichi Imaizumi [b], Hideka Shibuya [b], Junji Akimoto [c]

[a] National Institute of Advanced Industrial Science and Technology (AIST), 1-8-31 Midorigaoka, Ikeda, Osaka 563-8577, Japan
[b] Tanaka Chemical Corporation, 5-10 Shirakata, Fukui 910-131, Japan
[c] National Institute of Advanced Industrial Science and Technology (AIST), 1.1.1. Higashi, Tsukuba, Ibaraki 305-8565, Japan

## HIGHLIGHTS

- High-capacity Fe- and/or Ti-substituted $Li_2MnO_3$ positive electrode materials were prepared.
- They had higher initial cycle efficiency than 70% and higher specific capacity than 200 mAh $g^{-1}$.
- Beneficial electrochemical performance was accomplished using carbothermal reduction.
- They are attractive for use as positive electrode materials in large-scale lithium-ion batteries.

## ARTICLE INFO

*Article history:*
Received 15 July 2012
Received in revised form
18 August 2012
Accepted 21 August 2012
Available online 28 August 2012

*Keywords:*
Synthesis
Lithium batteries
Positive electrode material
Lithium iron oxide
Lithium manganese oxide
Carbothermal reduction

## ABSTRACT

Carbothermal reduction using sucrose was applied to Fe- and/or Ti-substituted $Li_2MnO_3$ positive electrode materials to improve their poor initial cycle efficiency (<60%) of 2.0–4.8 V. The initial cycle efficiency was improved from 53% to 68% for $Li_{1+x}(Ti_{0.5}Mn_{0.5})_{1-x}O_2$, 63%–72% for $Li_{1+x}(Fe_{0.3}Mn_{0.7})_{1-x}O_2$, or 62%–78% for $Li_{1+x}(Fe_{0.2}Ti_{0.2}Mn_{0.6})_{1-x}O_2$ by application of the carbothermal reduction process. All samples belong to 3.2 V class positive electrode material with high initial discharge capacity higher than 220 mAh $g^{-1}$. The shape change of discharge curve with cycle progression was suppressed for all reduced samples. The compositional, transition metal valence state, and structural and powder property changes occurring before and after carbothermal reduction processing were examined to construct the material design concept of attractive $Li_2MnO_3$-based positive electrode candidates using only naturally abundant and cheap elements (Ti and Fe) as constituent metals.



## 1. Introduction

Among constituent materials of lithium-ion batteries, the positive electrode material is most important because its electrochemical properties dictate the operating voltage and capacity of the battery. With expansion of the applications of the lithium-ion batteries to vehicle installation for EV or PHEV and to energy storage for renewable energy, resource savings and cost reductions of the positive electrode material are necessary because material costs of positive electrode materials are higher than those of other constituent materials, and because most positive electrode materials contain rare metal elements such as Co and Ni.

Even though many oxide-based positive electrodes ($LiNi_{0.8}Co_{0.2}O_2$, $LiNi_{1/3}Mn_{1/3}Co_{1/3}O_2$, $LiMn_2O_4$) have been proposed for the application described above, Li-excess layered manganese oxide materials ($(1-\delta)LiMO_2 - \delta Li_2MnO_3$, $0 < \delta < 1$, $M = Ni_{1/2}Mn_{1/2}$ or $Ni_{1/3}Mn_{1/3}Co_{1/3}$) are attractive candidates showing specific capacity higher than 250 mAh $g^{-1}$ within the wider voltage range from 2.0 to 4.8 V [1–3]. Among the various transition metal ratios, $Li_{1.2}Co_{0.13}Ni_{0.13}Mn_{0.54}O_2$ has been known as an optimized composition showing high initial charge and discharge capacities (328 and 253 mAh $g^{-1}$) [4]. However, many problems (lack of initial reversibility, large capacity fading with cycle number, bad rate performance etc.) have been described in relation to practical use.

* Corresponding author. Tel.: +81 727 51 9618; fax: +81 727 51 9714.
*E-mail address:* m-tabuchi@aist.go.jp (M. Tabuchi).

0378-7753/$ – see front matter © 2012 Elsevier B.V. All rights reserved.
http://dx.doi.org/10.1016/j.jpowsour.2012.08.055

The charge–discharge behavior of this material, which is rather complex, is mainly attributable to participation of the $Li_2MnO_3$ component as an electrochemically active material. While Li extraction and insertion reactions originating from the $LiMO_2$ component occurred between 3.5 and 4.4 V, $Li_2O$ extraction from $Li_2MnO_3$ occurred at voltages higher than 4.5 V on charging. In addition, Li insertion to "$Li_2O$-extracted $MnO_2$" component reactions occurred at voltages lower than 3.5 V on discharging [1,2,5]. The $Li_2MnO_3$ converts to spinel phase with increasing cycle number [6]. The thick passivation layer on the active material formed [7] and $O_2$ gas evolution occurred on initial charging at voltages higher than 4.5 V [8]. To optimize the electrochemical performance, setting $Li_2MnO_3$ content, $\delta$ in $(1-\delta)LiMO_2-\delta Li_2MnO_3$ solid solution is extremely important, as shown in Table 1 [2,3]. With increasing $Li_2MnO_3$ content, although the specific capacity increased drastically, other electrochemical characteristics became poor. In addition, special care is necessary for synthetic procedures because complete mixing of two or three transition metals is difficult by a simple solid-state reaction, and the discharge capacity of $Li_2MnO_3$ increased by reducing the primary particle size, which can be accomplished by lowering the calcination temperature [9]. These facts show that the material design concept to control electrochemical performance for the $(1-\delta)LiMO_2-\delta Li_2MnO_3$ remains under development.

From about ten years ago, we started to develop solid solutions of three kinds: Fe [10,11], Ti [12], and Fe and Ti [13] substituted $Li_2MnO_3$-positive electrode materials. These materials are attractive candidates for use in large lithium-ion batteries because they contain only inexpensive and naturally abundant transition metal elements. However, they had poor electrochemical performance. Particularly, the initial cycle efficiency was less than ca. 74% and the average discharge voltage was around 3.0 V (1.5–4.8 V) at room temperature [14]. For practical use, the initial cycle efficiency must be greater than 80% under a narrower voltage range (2.0–4.8 V). While we proposed Fe- and Ni-substituted $Li_2MnO_3$ ($Li_{1+x}(Fe_{0.2}Ni_{0.2}Mn_{0.6})_{1-x}O_2$) [15] as a new Co-free positive electrode material having high initial average discharge voltage 3.5 V at voltages of 2.0–4.8 V, a challenge to improve the poor electrochemical performance for the Fe- and/or Ti-substituted $Li_2MnO_3$ is necessary for the additional development of large-scale lithium-ion batteries.

As described in this paper, we sought to reduce the valence state of manganese using a carbothermal reduction method to obtain high initial cycle efficiency of greater than 80% in the voltage range of 2.0–4.8 V. The material design concept constructed from the change in valence state of manganese ion at the 1 cycled state; some manganese ions were reduced slightly from 4 + to 3 + state [1,2,5] and most $Li_2MnO_3$-based positive electrode materials have high cycle efficiency of greater than 95% after the second cycle. As Table 1 shows, partial reduction of $Mn^{4+}$ ion corresponds to a decrease in $\delta$ for $(1-\delta)LiMO_2-\delta Li_2MnO_3$ solid solution. Therefore we can expect to improve the cycle performance and raise the average discharge voltage (>3 V). Even though a similar approach was described in previous reports in the literature [2,16,17], the reduction method and target material differed. The carbothermal reduction method was used mainly for improvement of the rate capability of various positive electrode materials [18–20].

**Table 1**
Change in trends of the average valence state of constituent metals, and electrochemical data with increasing $Li_2MnO_3$ contents ($\delta$) for $(1-\delta)LiMO_2-\delta Li_2MnO_3$ ($M = Ni_{1/3}Mn_{1/3}Co_{1/3}$ [2] or $Ni_{1/2}Mn_{1/2}$ [3]) positive electrode materials reported previously.

| $Li_2MnO_3$ content, $\delta$ | $\delta < 0.5$ ($LiMO_2$ at $\delta = 0$) | $\delta > 0.5$ ($Li_2MnO_3$ at $\delta = 1$) |
|---|---|---|
| Li content | Small | Large |
| Average valence state of constituent metals | Less than 3.5+ | Greater than 3.5+ |
| Specific capacity | 150–200 mAh $g^{-1}$ | 250–300 mAh $g^{-1}$ |
| Initial cycle efficiency | 80–90% | 50–60% |
| Average discharge voltage | >3.5 V | <3.5 V |
| Cycle performance | Good | Bad |

## 2. Experimental

All samples (0.25 mol/batch) were synthesized using four-step processes comprising coprecipitation, hydrothermal reaction, calcination in air, and carbothermal reduction in an inert atmosphere. First, the mixed metal aqueous solution at a target transition metal ratio was prepared using $Fe(NO_3)_3\cdot 9H_2O$ (99.9%; Wako Pure Chemical Industries), $MnCl_2\cdot 4H_2O$ (99.0%; Wako Pure Chemical Industries), 30% $Ti(SO_4)_2$ solution (reagent grade; Wako Pure Chemical Industries), and distilled water (500 ml). The mixed metal solution was dropped into lithium hydroxide solution, which consists of 60 g of LiOH, and 1000 ml of distilled water to produce a mixed metal precipitate. The precipitate was aged by air bubbling treatment overnight.

After the aging process, the mixed metal precipitate was recovered by filtration process as a wet cake. The cake was mixed with 100 ml of distilled water, 50 g of $LiOH\cdot H_2O$, and 50 g of $KClO_3$ (oxidizer) into a PTFE beaker for hydrothermal treatment. The hydrothermal reaction time was 5 h at 220 °C into an autoclave. The product was washed repeatedly with distilled water to eliminate residual salts. Then the filtrated product was mixed with aqueous solution (100 ml) including 1/8 mol of $LiOH\cdot H_2O$ before drying at 100 °C overnight.

The dried mixture was calcined at 650 °C for 20 h in air after pulverization. The calcined product was dispersed in aqueous solution including sucrose. The amount of sucrose was adjusted to 0.1 M times of carbon per 1 batch. The dried mixture was calcined at 500 °C or 600 °C depending on the target metal ratio for 1 h under $N_2$ flow after pulverization (carbothermal reduction process). The products were purified by washing with distilled water, filtration, and drying at 100 °C for applying various characterization methods as well as electrochemical measurements. To examine the effects of carbothermal reduction, the reference samples were prepared separately by washing products with distilled water, filtration and by drying at 100 °C after the calcination described above at 650 °C in air.

The sample quality was checked using X-ray diffraction (XRD) measurements. For X-ray Rietveld analysis, Si powder (SRM 640c) was used as an external standard for calibrating the diffraction angle. The XRD data were collected between 10° and 125° of the $2\theta$ angles under monochromatized CuK$\alpha$ radiation using an X-ray diffractometer (Rotaflex RU-200B/RINT; Rigaku). A split pseudo-Voigt profile function was selected for each XRD peak fitting. A computer program (RIETAN-2000 [21]) was used for X-ray Rietveld analysis. The Li, Ti, Fe, and Mn elemental analyzes were performed using inductively coupled plasma (ICP) emission spectroscopy and average valence state of transition metals except for Ti was analyzed through iodometric titration. The carbon content was estimated using a CS analyzer (EMIA-320V2; Horiba). The Brunauer–Emmett–Teller (BET) surface area was measured and used as specific surface area (SSA) data. The particle size distribution was collected for 0.5–350 μm (Aerotrac SPR7340; Nikkiso). The validity of the obtained particle size distribution was confirmed using a standard powder (GBM-20; The Association of Powder Process Industry & Engineering, Japan) with average particle size of 22 ± 1.0 μm.

The valence state analysis of Mn or Ti ions was conducted using corresponding metal K-edge X-ray absorption near edge structure (XANES) measurements. These spectra were obtained in

**Table 2**
Li, Ti, Fe, and Mn contents, specific surface area (SSA) and average particle size ($D_{50}$) for Ti- and/or Fe-substituted $Li_2MnO_3$ positive electrode materials ($Li_{1+x}(Fe_yTi_zMn_{1-y-z})_{1-x}O_2$, $0 < x < 1/3$, $0 < y$ and/or $z \leq 0.5$).

| Nominal chemical formula of sample (sample name) | C (wt%) | Li (wt%) | Ti (wt%) | Mn (wt%) | Fe (wt%) | $Li_{1+x}(Fe_yTi_zMn_{1-y-z})_{1-x}O_2$ | | | | |
|---|---|---|---|---|---|---|---|---|---|---|
| | | | | | | $x$ | $y$ | $z$ | SSA/$m^2\ g^{-1}$ | $D_{50}$/μm |
| $Li_{1+x}(Ti_{0.5}Mn_{0.5})_{1-x}O_2$, after reduction, (R-TM) | 0.31 | 10.6 | 22.3 | 23.8 | – | 0.259 | – | 0.518 | 13.9 | 8.6(3) |
| $Li_{1+x}(Ti_{0.5}Mn_{0.5})_{1-x}O_2$, before reduction, (TM) | 0.14 | 11.6 | 21.5 | 23.2 | – | 0.315 | – | 0.515 | 23.0 | 8.4(4) |
| $Li_{1+x}(Fe_{0.3}Mn_{0.7})_{1-x}O_2$, after reduction, (R-FM) | 0.40 | 9.19 | – | 35.1 | 14.4 | 0.194 | 0.288 | – | 25.7 | 9.9(2) |
| $Li_{1+x}(Fe_{0.3}Mn_{0.7})_{1-x}O_2$, before reduction, (FM) | 0.25 | 10.3 | – | 32.9 | 14.1 | 0.270 | 0.297 | – | 26.7 | 9.9(1) |
| $Li_{1+x}(Ti_{0.2}Fe_{0.2}Mn_{0.6})_{1-x}O_2$, after reduction, (R-FMT) | 0.33 | 9.36 | 8.76 | 29.8 | 10.3 | 0.194 | 0.203 | 0.201 | 25.2 | 7.7(5) |
| $Li_{1+x}(Ti_{0.2}Fe_{0.2}Mn_{0.6})_{1-x}O_2$, Before reduction, (FMT) | 0.22 | 10.8 | 8.66 | 28.7 | 9.91 | 0.278 | 0.201 | 0.205 | 24.6 | 8.2(3) |

transmission mode using a laboratory-type X-ray spectrometer (EXAC-820; Technos) at 293 K. As reference samples, $LiMnO_2$ (orthorhombic form), $Li_2MnO_3$, Ti foil, $Ti_2O_3$, and $Li_2TiO_3$ were used. The $^{57}Fe$ Mössbauer spectra were recorded at room temperature (Model 222B; Topologic Systems); α-Fe was used for velocity calibration. Observed spectra were fitted to peaks with a Lorenzian line shape using a computer program (Mosswin 3.0). The magnetic field dependence of magnetization ($\sigma$) was measured at room temperature using a vibrating sample magnetometer (VSM; Riken Denshi) between −1 T and +1 T $(NH_4)_2Mn(SO_4)_2 \cdot 6H_2O$ was selected as the reference material of magnetization.

The electrochemical data for the samples were collected using a coin-type lithium-half cell (HS flat-cell; Hohsen). A pellet type positive electrode was made by adding a small amount of PTFE powder (0.5 mg) to a mixture of active material (5 mg) and acetylene black (5 mg). A typical liquid electrolyte was selected (1 M $LiPF_6$ in ethylene carbonate (EC) and dimethyl carbonate (DMC) mixed solvent (3:7 in volume ratio), Kishida Chemical). Lithium metal foil (Honjo Metal) was used as the negative electrode material. A cell was first charged to 4.8 V and then discharged to 2.0 V under a galvanostatic condition (40 mA $g^{-1}$) at 30 °C. Only at the end of charging was the cell was kept at 4.8 V until decreasing smaller current density to 10 mA $g^{-1}$.

Discharge properties was taken under high current densities of 40–3600 mA $g^{-1}$ at 30 °C after galvanostatic charging (40 mA $g^{-1}$) in the same voltage range. The cell cycled once galvanostatically at 40 mA $g^{-1}$ and 30 °C to compensate for the deviation of state of charge (SOC) originating from lowering of the discharge capacity under high current density. Same SOC adjustment procedures were used for examination of the discharge characteristics at 0 and −20 °C after charging at 40 mA $g^{-1}$.

## 3. Results and discussion

We select three systems, Ti-, Fe- or Fe and Ti-substituted $Li_2MnO_3$ as shown in Table 2. Among them, the Ti-substituted $Li_2MnO_3$ (TM) systems was pick up firstly, since clear change against $Li_2MnO_3$ component by carbothermal reduction was observed. Fe-substituted $Li_2MnO_3$ (FM) and Fe and Ti-substituted $Li_2MnO_3$ systems was explained after TM systems, because the carbothermal reduction process was still effective with presence of Fe ion or not. Addition of Ti and/or Fe ions into $Li_2MnO_3$ structure (above 30% to total transition metal content) was necessary to get homogenous sample after carbothermal reduction. The application of carbothermal reduction process to end member, $Li_2MnO_3$ was failed, because of the formation of mixture with orthorhombic $LiMnO_2$.

### 3.1. Differences in chemical composition, structure, valence states of Ti and Mn ions, and electrochemical properties before (TM) and after carbothermally reduced (R-TM) Ti-substituted $Li_2MnO_3$ samples (TM system)

The XRD patterns before (TM) and after carbothermally reduced (R-TM) samples are presented in Fig. 1 for Ti-substituted $Li_2MnO_3$ (nominal composition $Li_{1+x}(Ti_{0.5}Mn_{0.5})_{1-x}O_2$, $0 < x < 1/3$). All XRD peaks for each sample were indexed only by the unit-cell of end member, $Li_2MnO_3$ with monoclinic layered rock-salt structure ($C2/m$, [22]) because of the presence of broad peak from $2\theta = 20$–$25°$ originated from incomplete honeycomb-lattice ordering of Li, Ti, and Mn ions in the transition metal layer [7]. The reduction temperature was kept at 600 °C because cubic rock-salt $Li_2TiO_3$

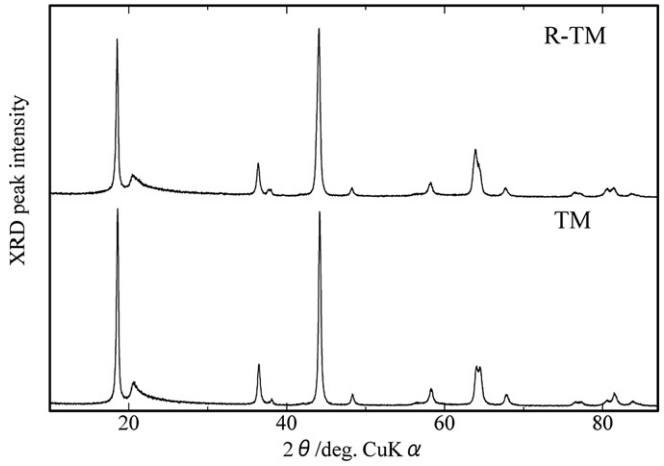


**Fig. 1.** X-ray diffraction patterns of before (TM sample) and after carbothermally reduced Ti-substituted $Li_2MnO_3$ (R-TM sample, nominal composition $Li_{1+x}(Ti_{0.5}Mn_{0.5})_{1-x}O_2$, $0 < x < 1/3$).

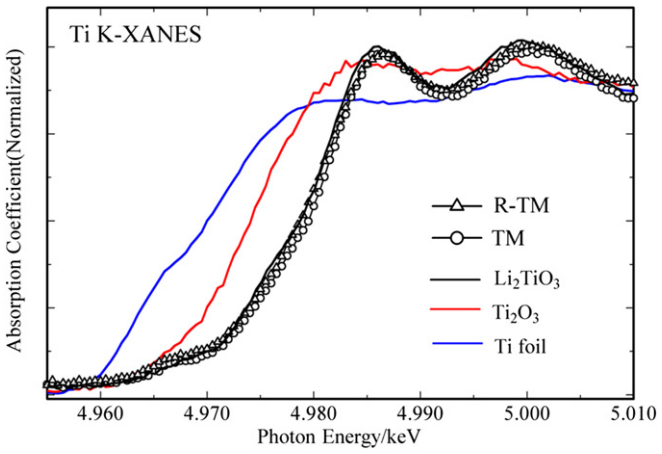


**Fig. 2.** Ti K-edge X-ray absorption spectra for of before (TM sample) and after carbothermally reduced Ti-substituted $Li_2MnO_3$ (R-TM sample, nominal composition $Li_{1+x}(Ti_{0.5}Mn_{0.5})_{1-x}O_2$, $0 < x < 1/3$). Three reference materials, Ti foil, $Ti_2O_3$, and $Li_2TiO_3$ powders were selected to estimate the valence state of Ti ion.

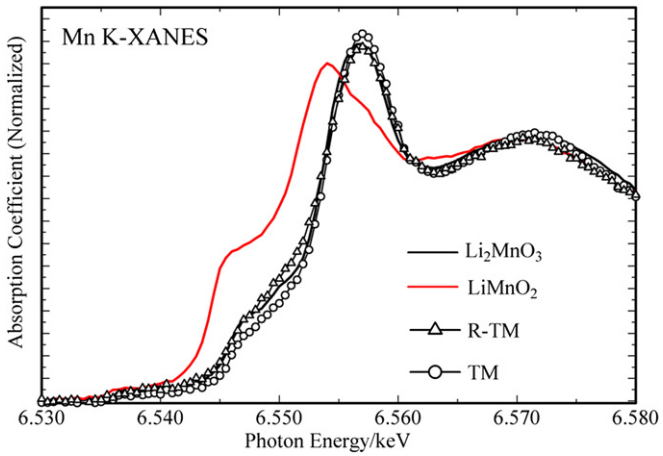


**Fig. 3.** Mn K-edge X-ray absorption spectra for of before (TM sample) and after carbothermally reduced Ti-substituted $Li_2MnO_3$ (R-TM sample, nominal composition $Li_{1+x}(Ti_{0.5}Mn_{0.5})_{1-x}O_2$, $0 < x < 1/3$). Three reference materials, $LiMnO_2$, and $Li_2MnO_3$ powders were selected to estimate the Mn ion valence state.

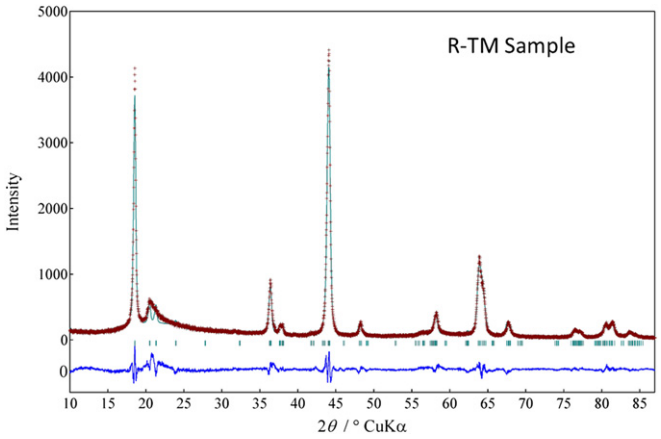


**Fig. 4.** Oberved (+) and calculated (solid line) X-ray diffraction patterns for R-TM sample. The difference between them was shown below the patterns with same scale.

phase ($Fm\bar{3}m$) coexisted with monoclinic $Li_2MnO_3$ by raising the reduction temperature to a temperature higher than 700 °C.

The chemical composition of the R-TM sample differs from that of the TM sample, as shown in Table 2, though the Ti/(Ti + Mn) ratio, $z$ (0.52) was close to the nominal one (0.50) for both samples. Even though the Li content was reduced, the Ti and Mn contents were increased after applying carbothermal reduction processes. The average valence state of Mn ion for the R-TM sample (3.81) was smaller than that (3.99) for the TM sample by iodometric titration. The fact means that the $x$ value in $Li_{1+x}(Ti_{0.5}Mn_{0.5})_{1-x}O_2$ decreased by carbothermal reduction if no oxygen vacancy was formed [23]. Carbon contents for the R-TM sample were slightly higher than that for TM (Table 2). The difference in carbon contents between them was small (<0.2%).

The Ti and Mn K-edge XANES spectra for R-TM and TM samples (Figs. 2 and 3) are overlapped to those for $Li_2TiO_3$ and $Li_2MnO_3$, indicating that a majority of Ti and Mn ions are the tetravalent state as expected from iodometric titration result for average Mn valence state. No reduction behavior was detected for Ti ion after carbothermal reduction. These trends correspond to the formation of $(1-\delta)LiMnO_2-\delta Li_2(Mn,Ti)O_3$ solid solution (R-TM sample) from $Li_2(Mn,Ti)O_3$ (TM sample) and the R-TM sample would have better electrochemical performance than that for the TM sample, as might be inferred from Table 1.

The lattice parameters and average transition metal occupancy in Li ($d$) and transition metal ($e$) layers for respective chemical formulas are presented in Table 3 using the X-ray Rietveld analysis (Fig. 4 for R-TM sample). The observed lattice parameters ($a$, $b$, $c$, and $V$) for the TM sample are larger than those for the end member $Li_2MnO_3$ ($a$ = 4.937(1) Å, $b$ = 8.532(1) Å, and $c$ = 5.030(2) Å and $V$ = 199.77 Å$^3$ [22]), indicating the substitution of large $Ti^{4+}$ (0.605 Å) ion for a small $Mn^{4+}$ (0.530 Å) one into $Li_2MnO_3$ structure. The $a$, $b$, and $c$ parameters for R-TM sample were larger than those for the TM one. That fact reflects the formation of large $Mn^{3+}$ ion (0.645 Å), as expected from iodometric titration results.

The average transition metal occupancy in Li ($d$) and transition metal ($e$) layers and their sum ($d + e$) per chemical formula are also presented in Table 3. The $d$ and $d + e$ values for R-TM sample were higher than those for TM, which correspond to transition metal disordering and valence state reduction of the transition metal occurring by carbothermal reduction, respectively. Cation disordering might hamper the improvement of electrochemical properties because fast Li diffusion is impeded by the existence of the transition metal ion in Li layer.

Electrochemical data for the R-TM sample were compared with those for the TM one, as shown in Table 4 and Fig. 5. The R-TM sample exhibited higher initial cycle efficiency and lower capacity fading than the TM one without lowering the initial discharge capacity and energy density. The results depict the validity of applying the carbothermal reduction process. The difference in initial charge curves was detected between them. The R-TM sample had larger initial charge capacity below 4.4 V and shorter $Li_2O$ extraction plateau than the other had. This suggests that the reduced Mn ions oxidized below 4.4 V and act as an activated cation like Cr, Fe, Ni or Co ion during initial charging process for $Li_2MnO_3$-based positive electrode material. The $Ti^{4+}$ ion act as active $Li_2TiO_3$ component for $Li_2O$ extraction part, like $Li_2MnO_3$ one, since TM sample has high initial charge capacity like $Li_2MnO_3$.

The shape of initial, tenth, and 20th discharge curves for R-TM sample was also changed from that for TM one below 3.5 V. The variation of charge and discharge curves was anticipated from

**Table 3**
Refined crystallographic parameters obtained using X-ray Rietveld analysis for Ti- and/or Fe-substituted $Li_2MnO_3$ positive electrode material using a layered rock-salt unit cell. The unit cell was constructed from the monoclinic $Li_2MnO_3$ structure ($C2/m$).

| Nominal chemical formula of sample (sample name) | $a$/Å | $b$/Å | $c$/Å | $\beta$/° | $V$/Å$^3$ | $(Li_{1-d}M_d)_{Li}[Li_{1-e}M_e]_{M-Li}O_2$[a] | | |
|---|---|---|---|---|---|---|---|---|
| | | | | | | $d$ | $e$ | $d + e$ |
| $Li_{1+x}(Ti_{0.5}Mn_{0.5})_{1-x}O_2$, after reduction, (R-TM) | 5.0241(12) | 8.6538(15) | 5.0594(9) | 109.285(19) | 207.63(7) | 0.114(7) | 0.569(7) | 0.683(14) |
| $Li_{1+x}(Ti_{0.5}Mn_{0.5})_{1-x}O_2$, before reduction, (TM) | 5.0086(15) | 8.6485(19) | 5.0489(11) | 109.25(2) | 206.47(8) | 0.045(6) | 0.581(7) | 0.626(13) |
| $Li_{1+x}(Fe_{0.3}Mn_{0.7})_{1-x}O_2$, after reduction, (R-FM) | 4.9722(13) | 8.5617(15) | 5.0287(11) | 109.13(2) | 202.25(8) | 0.086(3) | 0.651(8) | 0.737(8) |
| $Li_{1+x}(Fe_{0.3}Mn_{0.7})_{1-x}O_2$, before reduction, (FM) | 4.9699(16) | 8.574(2) | 5.0325(12) | 109.16(3) | 202.56(9) | 0.065(2) | 0.646(7) | 0.721(7) |
| $Li_{1+x}(Ti_{0.2}Fe_{0.2}Mn_{0.6})_{1-x}O_2$, after reduction, (R-FMT) | 5.0060(12) | 8.6209(15) | 5.0419(10) | 109.19(2) | 205.50(7) | 0.089(2) | 0.637(7) | 0.726(7) |
| $Li_{1+x}(Ti_{0.2}Fe_{0.2}Mn_{0.6})_{1-x}O_2$, before reduction, (FMT) | 5.0006(14) | 8.6174(17) | 5.0385(11) | 109.21(2) | 205.03(8) | 0.075(2) | 0.620(7) | 0.695(7) |

[a] The chemical formula was used for calculating transition metal ($M$) contents on Li layer ($d$) and $M$-Li layer ($e$). The $d$ and $e$ values were calculated from the $M$ occupancy ($g$) on four different crystallographic sites (2$c$, 4$h$, 2$b$, and 4$g$ sites), respectively, using the equations $d = (g_{2c} + 2g_{4h})/3$ and $e = (g_{2b} + 2g_{4g})/3$.

**Table 4**
Electrochemical charge and discharge characteristics for Li/(Ti- and/or Fe-substituted $Li_2MnO_3$) cells at 30 °C. Data of cells operated between 2.0 and 4.8 V under a fixed current density, 40 mA $g^{-1}$. Charging remained at the higher upper limit voltage (4.8 V) until reduction of the current density to 10 mA $g^{-1}$ during all charging runs.

| Nominal chemical formula of sample (sample name) | $Q_{1c}$/mAh $g^{-1}$ | $Q_{1d}$/mAh $g^{-1}$ | $Q_{1d}/Q_{1c}$ | $V_{1d}/V$ | $V_{1d}\cdot Q_{1d}$/mWh $g^{-1}$ | $Q_{20d}$/mAh $g^{-1}$ | $Q_{20d}/Q_{1d}$ |
|---|---|---|---|---|---|---|---|
| $Li_{1+x}(Ti_{0.5}Mn_{0.5})_{1-x}O_2$, after reduction, (R-TM) | 324 | 219 | 0.677 | 3.24 | 712 | 192 | 0.877 |
| $Li_{1+x}(Ti_{0.5}Mn_{0.5})_{1-x}O_2$, before reduction, (TM) | 400 | 214 | 0.534 | 3.22 | 688 | 140 | 0.654 |
| $Li_{1+x}(Fe_{0.3}Mn_{0.7})_{1-x}O_2$, after reduction, (R-FM) | 307 | 222 | 0.723 | 3.26 | 723 | 167 | 0.752 |
| $Li_{1+x}(Fe_{0.3}Mn_{0.7})_{1-x}O_2$, before reduction, (FM) | 347 | 220 | 0.633 | 3.22 | 707 | 161 | 0.732 |
| $Li_{1+x}(Ti_{0.2}Fe_{0.2}Mn_{0.6})_{1-x}O_2$, after reduction, (R-FMT) | 307 | 239 | 0.779 | 3.25 | 776 | 183 | 0.766 |
| $Li_{1+x}(Ti_{0.2}Fe_{0.2}Mn_{0.6})_{1-x}O_2$, before reduction, (FMT) | 358 | 221 | 0.619 | 3.20 | 707 | 153 | 0.692 |

$Q_{1c}$, initial charge capacity; $Q_{1d}$, initial discharge capacity; $Q_{1d}/Q_{1c}$, initial cycle efficiency; $V_{1d}$, average initial discharge voltage; $V_{1d}\cdot Q_{1d}$, initial discharge energy density; $Q_{20d}$, 20th discharge capacity.

chemical composition changes originating from the partial reduction of the $Mn^{4+}$ ion in R-TM sample (decrease in $Li_2MnO_3$ content, $\delta$), as shown in Table 1 [2,3].

Bommel and Dahn reported that $Li[Li_{1/9}Ni_{1/3}Mn_{5/9}]O_2$ with small average particle size (3 μm) exhibited higher specific capacity than that for the large one (8 μm) [24]. The average particle size values ($D_{50}$) are the same for both samples within experimental error, as shown in Table 2. Therefore, the particle size distribution is not an important factor that is responsible for the present result.

The suppression of capacity fading for R-TM sample might be explained by its smaller SSA value than that for the TM sample (see Table 2) as well as the case of Fe-substituted $Li_2MnO_3$. The 50% Fe-substituted $Li_2MnO_3$ sample with small SSA values less than 22 $m^2$ $g^{-1}$ exhibited better cycle retention [25]. However, a small SSA value gave poor initial cycle efficiency for Fe-substituted $Li_2MnO_3$ [25] and Fe- and Ni-substituted $Li_2MnO_3$ [15]. For that reason, the initial cycle efficiency improvement for the R-TM sample does not originate from the change in the SSA value.

In the $LiNi_{1/2}Mn_{1/2}O_2$ positive electrode material, the cation disordering trend (increase in $d$ at Table 3) led to poor initial cycle efficiency and bad rate performance [26]. In our case, better initial cycle performance was obtained for R-TM sample in spite of its high transition metal content in Li layer, $d$, suggesting that cation disordering is not as important factor for our material as the SSA value is.

In Fig. 6 and Table 5, discharge capacities for the R-TM sample were higher than those for TM until 3600 mA $g^{-1}$ in (a) and −20 °C in (b). This result cannot be explained by the change in SSA data [14] and cation distribution [26]. As a summary, partial reduction of $Mn^{4+}$ ion using the carbothermal reduction process is an effective means to synthesize Ti-substituted $Li_2MnO_3$ with attractive electrochemical performance of 2.0–4.8 V.

### 3.2. Differences in chemical composition, structure, valence states of Mn and Fe, and electrochemical properties before (FM) and after carbothermally reduced (R-FM) Fe-substituted $Li_2MnO_3$ samples (FM system)

To extend the material design concept described above to other systems, we select Fe-substituted $Li_2MnO_3$ ($Li_{1+x}(Fe_{0.3}Mn_{0.7})_{1-x}O_2$) as the next target material (R-FM and FM samples). Almost the same XRD patterns were collected before (FM) and after carbothermal reduction at 500 °C (Fig. 7). Both samples were single-phase monoclinic $Li_2MnO_3$-type structure ($C2/m$). The SSA and $D_{50}$ values were almost identical to each other (Table 2). The increase in carbon content by application of carbothermal reduction was less than 0.2% (Table 2).

Magnetic field ($H$) dependence of magnetization ($\sigma$) was measured using VSM to estimate the amounts of magnetic impurities such as lithium ferrite $LiFe_5O_8$ with a spinel structure ($Fd\bar{3}m$, Fig. 8). $LiFe_5O_8$ is ferrimagnetic at temperatures below 670 °C. Its saturation magnetization ($\sigma_s$) is 65 $Gcm^3$ $g^{-1}$ at 20 °C [27]. Because the R-FM and FM samples were paramagnetic at room temperature from the doublet nature of $^{57}$Fe Mossbauer spectrum (Fig. 9), the detected saturation magnetization derived only from magnetic impurities. The $\sigma$–$H$ curve of FM sample was regarded as linearly dependent above 5 or below −5 kOe, indicating that the paramagnetic behavior and the shape of the curve was not linear between −5 and 5 kOe, which corresponds to a typical curve from magnetic impurities. The saturation magnetization data were calculated as the average value of two absolute intercept values at zero magnetic field resultant from two regression lines between 5 and 10 kOe and between −5 and −10 kOe. The saturation magnetization values were 0.0418(10) $Gcm^3$ $g^{-1}$ for FM and 0.0362(5) $Gcm^3$ $g^{-1}$ for R-FM

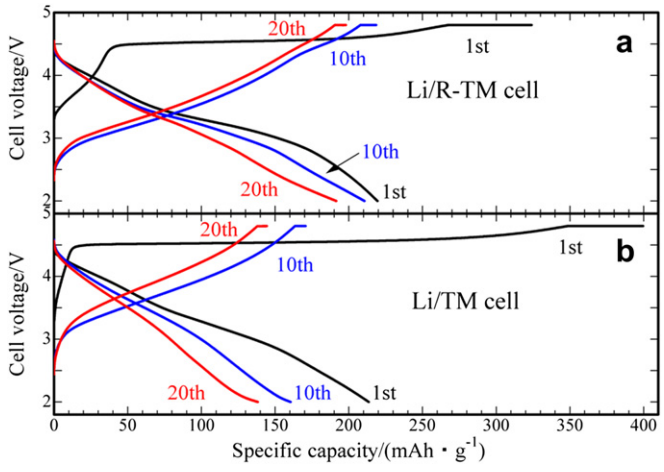


**Fig. 5.** Initial, tenth, and 20th charge and discharge curves for Li/R-TM sample (a) and Li/TM sample (b) cells at 30 °C. Current density was fixed at 40 mA $g^{-1}$.

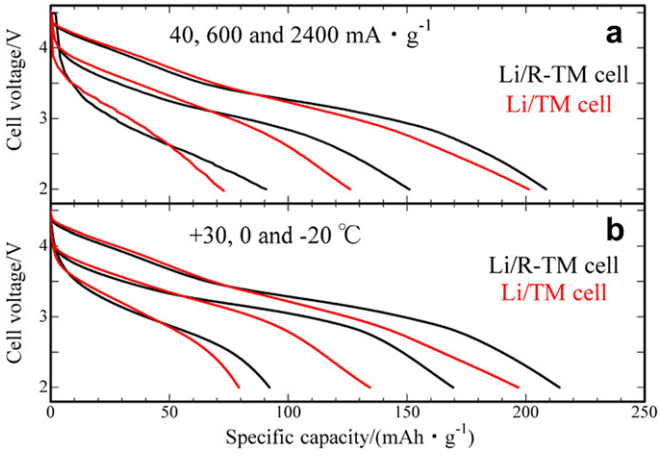


**Fig. 6.** High rate discharge characteristics for Li/R-TM sample and Li/TM sample cells at 30 °C under 40, 600, and 2400 mA $g^{-1}$ (a) and low-temperature discharge characteristics for them at 40 mA $g^{-1}$ under 30, 0, and −20 °C (b). Current density was fixed at 40 mA $g^{-1}$ and 30 °C on charging to 4.8 V before collecting discharge data.

**Table 5**
Electrochemical discharge characteristics from 4.8 to 2.0 V for Li/(Ti- and/or Fe-substituted $Li_2MnO_3$) cells under different current density and temperature at less than 30 °C at a fixed current density. The cells were charged and discharged between 2.0 and 4.8 V under a fixed current density of 40 mA $g^{-1}$ at 30 °C before charging to take all discharge characteristic data. Charging remained at the upper limit of voltage (4.8 V) until the current density was reduced to 10 mA $g^{-1}$.

| Nominal chemical formula of sample (sample name) | Discharge capacity under different current density/mAh $g^{-1}$ | | | | | | Discharge capacity under different temperatures/mAh $g^{-1}$ | | |
|---|---|---|---|---|---|---|---|---|---|
| | 40 mA $g^{-1}$ | 120 mA $g^{-1}$ | 600 mA $g^{-1}$ | 1200 mA $g^{-1}$ | 2400 mA $g^{-1}$ | 3600 mA $g^{-1}$ | 30 °C | 0 °C | −20 °C |
| $Li_{1+x}(Ti_{0.5}Mn_{0.5})_{1-x}O_2$, after reduction, (R-TM) | 209 | 182 | 151 | 128 | 91 | 61 | 214 | 169 | 92 |
| $Li_{1+x}(Ti_{0.5}Mn_{0.5})_{1-x}O_2$, before reduction, (TM) | 201 | 162 | 126 | 104 | 73 | 55 | 197 | 134 | 79 |
| $Li_{1+x}(Fe_{0.3}Mn_{0.7})_{1-x}O_2$, after reduction, (R-FM) | 210 | 193 | 164 | 137 | 93 | 67 | 215 | 164 | 103 |
| $Li_{1+x}(Fe_{0.3}Mn_{0.7})_{1-x}O_2$, before reduction, (FM) | 204 | 190 | 164 | 130 | 77 | 51 | 195 | 146 | 98 |
| $Li_{1+x}(Ti_{0.2}Fe_{0.2}Mn_{0.6})_{1-x}O_2$, after reduction, (R-FMT) | 235 | 213 | 183 | 157 | 106 | 73 | 232 | 178 | 116 |
| $Li_{1+x}(Ti_{0.2}Fe_{0.2}Mn_{0.6})_{1-x}O_2$, before reduction, (FMT) | 214 | 192 | 146 | 104 | 62 | 44 | 212 | 155 | 75 |

samples. If the magnetic impurity was only $LiFe_5O_8$, then the estimated $LiFe_5O_8$ contents were only 0.064 wt% for FM and 0.056 wt% for R-FM samples. This fact means that the contribution of magnetic impurities to both samples is negligibly small. The magnetization measurement is one of important characterization tool for Fe-substituted $Li_2MnO_3$, since detectable amount of magnetic impurity is quite low (less than 0.1 wt%) compared to XRD measurement.

Elemental analysis of both samples (Table 2) showed that the Li content was decreased and Fe and Mn contents were increased after carbothermal reduction in an analogous mode of TM system. The Fe content per chemical formula, $y$ was close to the nominal value (0.30). The average oxidation states of Fe and Mn were 3.68 for FM and 3.49 for R-FM samples. The transition metal contents on Li layer ($d$) and sum of transition metal occupancies per chemical formula ($d + e$) in Table 3 were increased by application of carbothermal reduction. These results indicate the formation of transition metal reduced sample with a cation-disordered layered rock-salt structure.

Similar Mn K-edge XANES spectra to Fig. 3 were collected for both samples. However, precise estimation of Mn valence state using only these spectra is difficult, as explained for Fig. 3. We estimate the valence state of the Fe ion from $^{57}$Fe Mössbauer spectra first. Then the Mn valence state was calculated by considering the Fe and Mn average valence state data above using iodometric titration, and Fe and Mn contents, $y$ and $1 - y$, respectively using elemental analysis. The observed $^{57}$Fe Mössbauer spectra (Fig. 9) were fitted by one or two symmetric doublets designated as A and B components with different isomer shift (IS) values. The main A (area fraction = 96%) and minor B (area fraction = 4%) components for FM sample had different IS values of +0.3450(10) and −0.120(17) mm $s^{-1}$, respectively. The spectrum of R-FM was fitted by only one doublet with +0.3402(8) mm $s^{-1}$ of IS value. From the IS values, A and B components were assigned as trivalent (IS = +0.33 mm $s^{-1}$) and tetravalent states (−0.11 mm $s^{-1}$) of Fe ions, respectively, from the previous result of $Li_{0.28}(Fe_{0.10}Ni_{0.90})_{1.06}O_2$ [28]. Stabilization of the high oxidation state Fe ions was accomplished by surrounding small $Mn^{4+}$ ions in a transition metal layer of Fe-substituted $Li_2MnO_3$ [29,30]. Assuming that the area fraction of each Fe component corresponds directly to average oxidation states of Fe ion, which were 3.04 for FM or 3.00 for R-FM samples. Calculated Mn oxidation state were 3.95 for FM sample and 3.67 for the R-FM one. The carbothermal reduction process can reduce both Fe and Mn ions for Fe-substituted $Li_2MnO_3$ materials.

The electrochemical cycle data of FM and R-FM samples are shown in Table 4 and Fig. 10. In the similar mode of the TM sample part, improvement of the initial cycle efficiency (from 63% to 72%) was observed by application of carbothermal reduction. Even though cycle fading behavior was not changed drastically, shape 10 and 20th discharge curves were similar to the initial one for the R-FM sample (Fig. 10(a)), different from the discharge curve shape change with cycle progression for FM one (Fig. 10(b)). High rate and low temperature discharge performance were improved above 2400 mA $g^{-1}$ (Fig. 11(a) and Table 5) and at 0 °C (Fig. 11(b) and Table 5). The electrochemical trend indicates that the carbothermally synthesized Fe-substituted $Li_2MnO_3$ material is also attractive as a positive electrode material when the cell operated between 2.0 and 4.8 V vs. $Li/Li^+$.

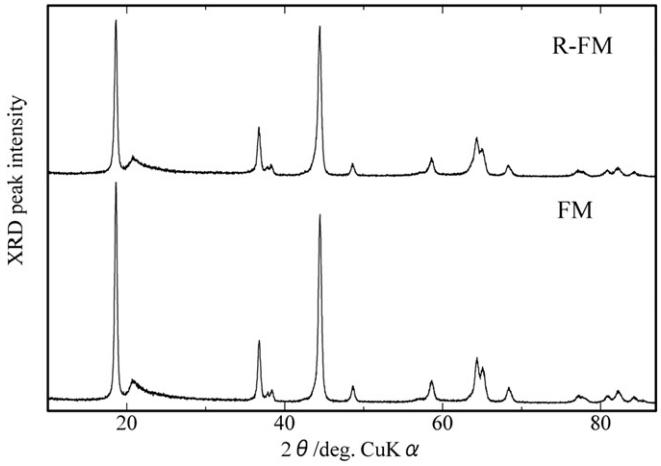


**Fig. 7.** X-ray diffraction patterns of before (FM sample) and after carbothermally reduced Fe substituted $Li_2MnO_3$ (R-FM sample, nominal composition $Li_{1+x}(Fe_{0.3}Mn_{0.7})_{1-x}O_2$, $0 < x < 1/3$).

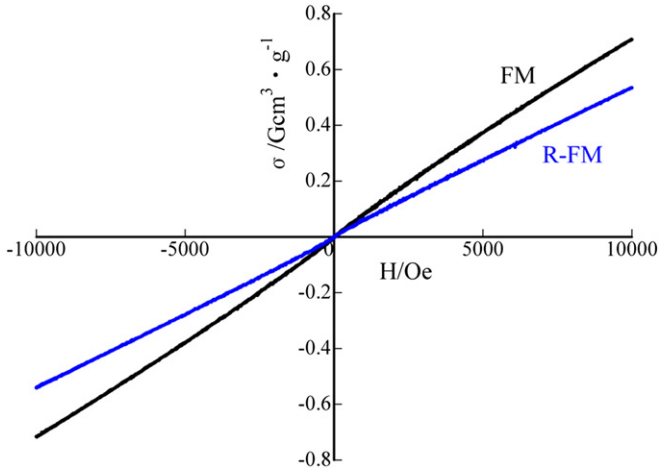


**Fig. 8.** Magnetic field ($H$) dependence of magnetization ($\sigma$) for FM and R-FM samples at 25 °C.

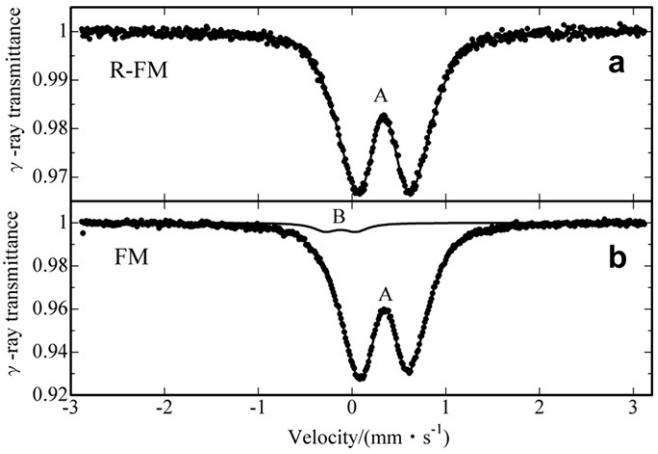


**Fig. 9.** Observed (●) and calculated (solid line) $^{57}$Fe Mössbauer spectra for R-FM (a) and FM samples (b) at room temperature. One or two symmetric doublets named A and B with different isomer shift values were used for fitting observed spectra depending on their shape.

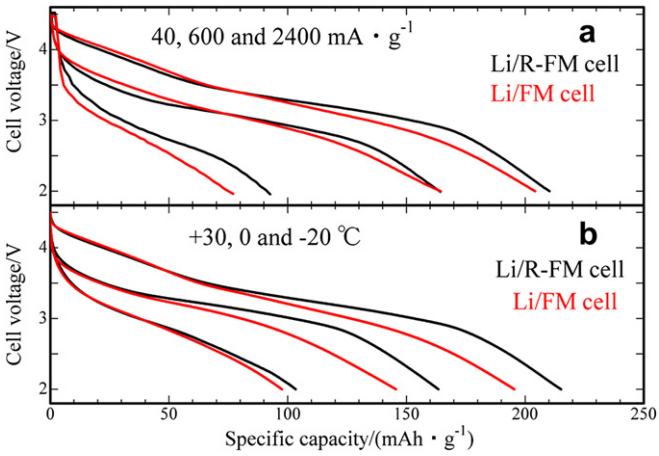


**Fig. 11.** High rate discharge characteristics for Li/R-FM sample and Li/FM sample cells at 30 °C under 40, 600, and 2400 mA $g^{-1}$ (a) and low-temperature discharge characteristics for them at 40 mA $g^{-1}$ under 30, 0, and −20 °C (b). Current density was fixed at 40 mA $g^{-1}$ and 30 °C on charging to 4.8 V before collecting discharge data.

### 3.3. *Differences in chemical composition, structure, valence states of Ti, Mn, and Fe, and electrochemical properties for before (FMT) and after carbothermally reduced (R-FMT) Fe- and Ti-substituted $Li_2MnO_3$ samples (FMT system)*

To find a more electrochemically attractive metal combination ratio, $Li_{1+x}(Fe_{0.2}Ti_{0.2}Mn_{0.6})_{1-x}O_2$ composition (FMT sample) was prepared for carbothermal reduction at 500 °C (R-FMT sample). The XRD patterns of both samples indicate the formation of a single phase of monoclinic $Li_2MnO_3$ phase (*C*2/*m*, Fig. 12). The SSA and $D_{50}$ values were almost mutually identical within experimental error (Table 2). The difference in carbon contents between both samples was less than 0.2%, as it was with other systems (Table 2). The nominal transition metal combination ratio was maintained until final products by Fe, Mn, and Ti elemental analysis (Table 2). The average oxidation state of Fe and Mn ions for R-FMT sample (3.56) is lower than that (3.67) of the FMT one by iodometric titration, as is the increase in *a*, *b*, and *c* lattice parameter values and lattice volume and transition metal occupancies (*d* and *e* values in Table 3) after applying carbothermal reduction. Fitting $^{57}$Fe Mössbauer spectra for both samples indicate that the average oxidation states were 3.05 for FMT and 3.00 for R-FMT samples. The average oxidation states of Mn ion were 3.99 for FMT 3.75 for R-FMT samples. The results presented above indicate the formation of Fe

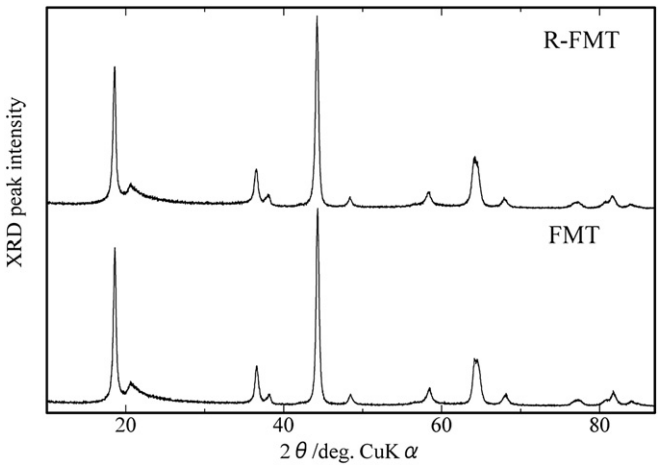


**Fig. 12.** X-ray diffraction patterns of before (FMT sample) and after carbothermally reduced Ti- and Fe-substituted $Li_2MnO_3$ (R-FMT sample, nominal composition $Li_{1+x}(Ti_{0.2}Fe_{0.2}Mn_{0.6})_{1-x}O_2$, $0 < x < 1/3$).

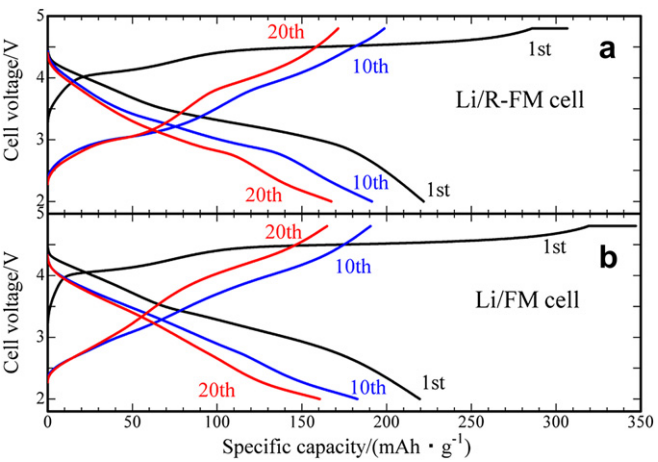


**Fig. 10.** Initial, tenth, and 20th charge and discharge curves for Li/R-FM sample (a) and Li/FM sample (b) cells at 30 °C. Current density was fixed at 40 mA $g^{-1}$.

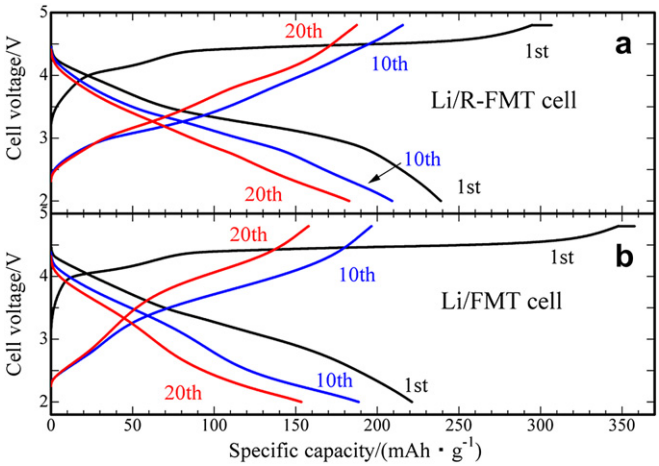


**Fig. 13.** Initial, tenth, and 20th charge and discharge curves for Li/R-FMT sample (a) and Li/FMT sample (b) cells at 30 °C. Current density was fixed at 40 mA $g^{-1}$.

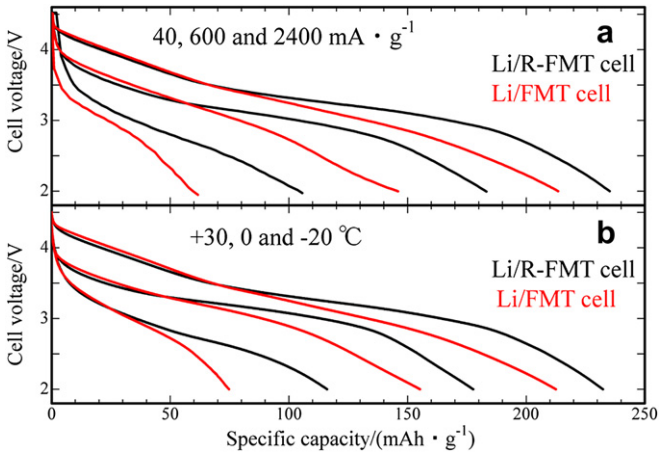


**Fig. 14.** High rate discharge characteristics for Li/R-FMT sample and Li/FMT sample cells at 30 °C under 40, 600, and 2400 mA $g^{-1}$ (a) and low temperature discharge characteristics for them at 40 mA $g^{-1}$ under 30, 0, and −20 °C (b). The current density was fixed at 40 mA $g^{-1}$ and 30 °C on charging to 4.8 V before collecting discharge data.

and Mn reduced R-FMT sample. No $Ti^{4+}$ ion reduction behavior was identified from Ti K-edge XANES spectra.

The electrochemical performance including initial cycle efficiency, average discharge voltage, energy density and cycle retention of discharge capacity was improved through carbothermal reduction processes (Table 4 and Fig. 13). The discharge characteristics under high current density (<3600 mA $g^{-1}$) or low temperature (<−20 °C) for R-FMT sample were better than those for FMT sample (Table 5 and Fig. 14). The R-FMT sample is an attractive positive electrode material from the standpoint of high rate and low-temperature performance.

## 4. Conclusion

Three metal combination systems, Ti-, Fe-, and Ti- and Fe-substituted $Li_2MnO_3$ are attractive 3.2–3.3 V class positive electrode materials by careful control not only of the transition metal combination ratio using coprecipitation–hydrothermal–calcination method but also the valence state of Mn and Fe through carbothermal reduction process. All can operate between 2.0 and 4.8 V as well as existing 3.5–3.7 V class systems such as Ni or Ni and Co substituted $Li_2MnO_3$ [2–4]. All reduced-samples had transition metal disordered structure. In spite of that, they exhibit better electrochemical charge and discharge performance as well as high-rate and low temperature discharge characteristics than those of transition metal-ordered and non-reduced samples. The fact suggests that efforts to prepare transition metal ordered sample may be meaningless to get the $Li_2MnO_3$ based positive electrode materials with better electrochemical performance. The formation of reduced Mn ion in reduced samples might be effective to improve their electrochemical performance. Although the average discharge voltage of our material is still low (<3.3 V), our proposed materials will be necessary to construct a large-scale lithium-ion battery since they contain only naturally abundant and cheap transition metal elements such as Ti, Fe, and Mn.

## Acknowledgments

MT expresses his gratitude to Prof. Tatsuya Nakamura of the University of Hyogo for fruitful discussions. This study was supported financially by a national project (Li-EAD project) of the Ministry of Economy, Trade and Industry (METI) and the New Energy and Industrial Technology Development Organization (NEDO).

## References

[1] M.M. Thackeray, S. Kang, C.S. Johnson, J.T. Vaughey, R. Benedek, S.A. Hackney, J. Mater. Chem. 17 (2007) 3112–3125.
[2] C.S. Johnson, N. Li, C. Lefief, J.T. Vaughey, M.M. Thackeray, Chem. Mater. 20 (2008) 6095–6106.
[3] Z. Lu, L.Y. Beaulieu, R.A. Donaberger, C.L. Thomas, J.R. Dahn, J. Electrochem. Soc. 149 (2002) A778–A791.
[4] Y. Wu, A. Manthiram, Electrochem. Solid-State Lett. 9 (2006) A221–A224.
[5] C.S. Johnson, J.-S. Kim, C. Lefief, N. Li, J.T. Vaughey, M.M. Thackeray, Electrochem. Commun. 6 (2004) 1085–1091.
[6] A.D. Robertson, P.G. Bruce, Chem. Mater. 15 (2003) 1984–1992.
[7] M. Jiang, B. Key, Y.S. Meng, C.P. Grey, Chem. Mater. 21 (2009) 2733–2745.
[8] A.R. Armstrong, M. Holzapfel, P. Novák, C.S. Johnson, S. Kang, M.M. Thackeray, P.G. Bruce, J. Am. Chem. Soc. 128 (2006) 8694–8698.
[9] D.Y.W. Yu, K. Yanagida, Y. Kato, H. Nakamura, J. Electrochem. Soc. 156 (2009) A417–A424.
[10] M. Tabuchi, H. Shigemura, K. Ado, H. Kobayashi, H. Sakaebe, H. Kageyama, R. Kanno, J. Power Sources 97-98 (2001) 415–419.
[11] M. Tabuchi, A. Nakashima, H. Shigemura, K. Ado, H. Kobayashi, H. Sakaebe, H. Kageyama, T. Nakamura, M. Kohzaki, A. Hirano, R. Kanno, J. Electrochem. Soc. 149 (2002) A509–A524.
[12] M. Tabuchi, Y. Nabeshima, T. Takeuchi, K. Tatsumi, Meeting Abstracts of the 49th Battery Symposium in Japan, Osaka, 2008, 2B08.
[13] M. Tabuchi, Y. Nabeshima, K. Ado, T. Takeuchi, M. Shikano, H. Kageyama, K. Tatsumi, Meeting Abstracts of the 47th Battery Symposium in Japan, Tokyo, 2006, 2D-19.
[14] M. Tabuchi, Y. Nabeshima, T. Takeuchi, K. Tatsumi, J. Imaizumi, Y. Nitta, J. Power Sources 195 (2010) 834–844.
[15] M. Tabuchi, Y. Nabeshima, T. Takeuchi, H. Kageyama, K. Tatsumi, J. Akimoto, H. Shibuya, J. Imaizumi, J. Power Sources 196 (2011) 3611–3622.
[16] J.S. Kim, C.S. Johnson, J.T. Vaughey, M.M. Thackeray, J. Power Sources 153 (2006) 258–264.
[17] A. Abouimrane, O.C. Compton, H. Deng, I. Belharouak, D.A. Dinkin, S.T. Nguyen, K. Amine, Electrochem. Solid-State Lett. 14 (2011) A126–A129.
[18] X.M.H. Li, X. Huang, Electrochem. Solid-State Lett. 9 (2006) A324–A327.
[19] J. Liu, Q. Wang, B. Reeja-Jayan, A. Manthiram, Electrochem. Commun. 12 (2010) 750–753.
[20] B.L. Cushing, J.B. Goodenough, Solid State Sci. 4 (2002) 1487–1493.
[21] F. Izumi, T. Ikeda, Mater. Sci. Forum 321–324 (2000) 198–203.
[22] P. Strobel, B. Lambert-Andron, J. Solid State Chem. 75 (1988) 90–98.
[23] K. Kubota, T. Kaneko, M. Hirayama, M. Yonemura, Y. Imanari, K. Nakane, R. Kanno, J. Power Sources 216 (2012) 249–255.
[24] A. Bommel, J.R. Dahn, Electrochem. Solid-State Lett. 13 (2010) A62–A64.
[25] M. Tabuchi, Y. Nabeshima, K. Ado, M. Shikano, H. Kageyama, K. Tatsumi, J. Power Sources 174 (2007) 554–559.
[26] K. Kang, Y.S. Meng, J. Bréger, C.P. Grey, G. Ceder, Science 311 (2006) 977–980.
[27] J. Smit, H.P.J. Wijn, Ferrites, International, Philips' Technical Library, Eindhoven, The Netherlands, 1965, Ch. 8.
[28] G. Prado, A. Rougier, L. Fournés, C. Delmas, J. Electrochem Soc. 147 (2000) 2880–2887.
[29] M. Tabuchi, A. Nakashima, K. Ado, H. Kageyama, K. Tatsumi, Chem. Mater. 17 (2005) 4668–4677.
[30] M. Tabuchi, K. Tatsumi, S. Morimoto, S. Nasu, T. Saito, Y. Ikeda, J. Appl. Phys. 104 (2008) 043909-1–043909-10.